

Supplement of Atmos. Chem. Phys., 16, 10847–10864, 2016  
<http://www.atmos-chem-phys.net/16/10847/2016/>  
doi:10.5194/acp-16-10847-2016-supplement  
© Author(s) 2016. CC Attribution 3.0 License.



*Supplement of*

## **Sensitivity of modelled sulfate aerosol and its radiative effect on climate to ocean DMS concentration and air–sea flux**

**Jan-Erik Tesdal et al.**

*Correspondence to:* Jan-Erik Tesdal (tesdal@ldeo.columbia.edu)

The copyright of individual parts of the supplement might differ from the CC-BY 3.0 licence.

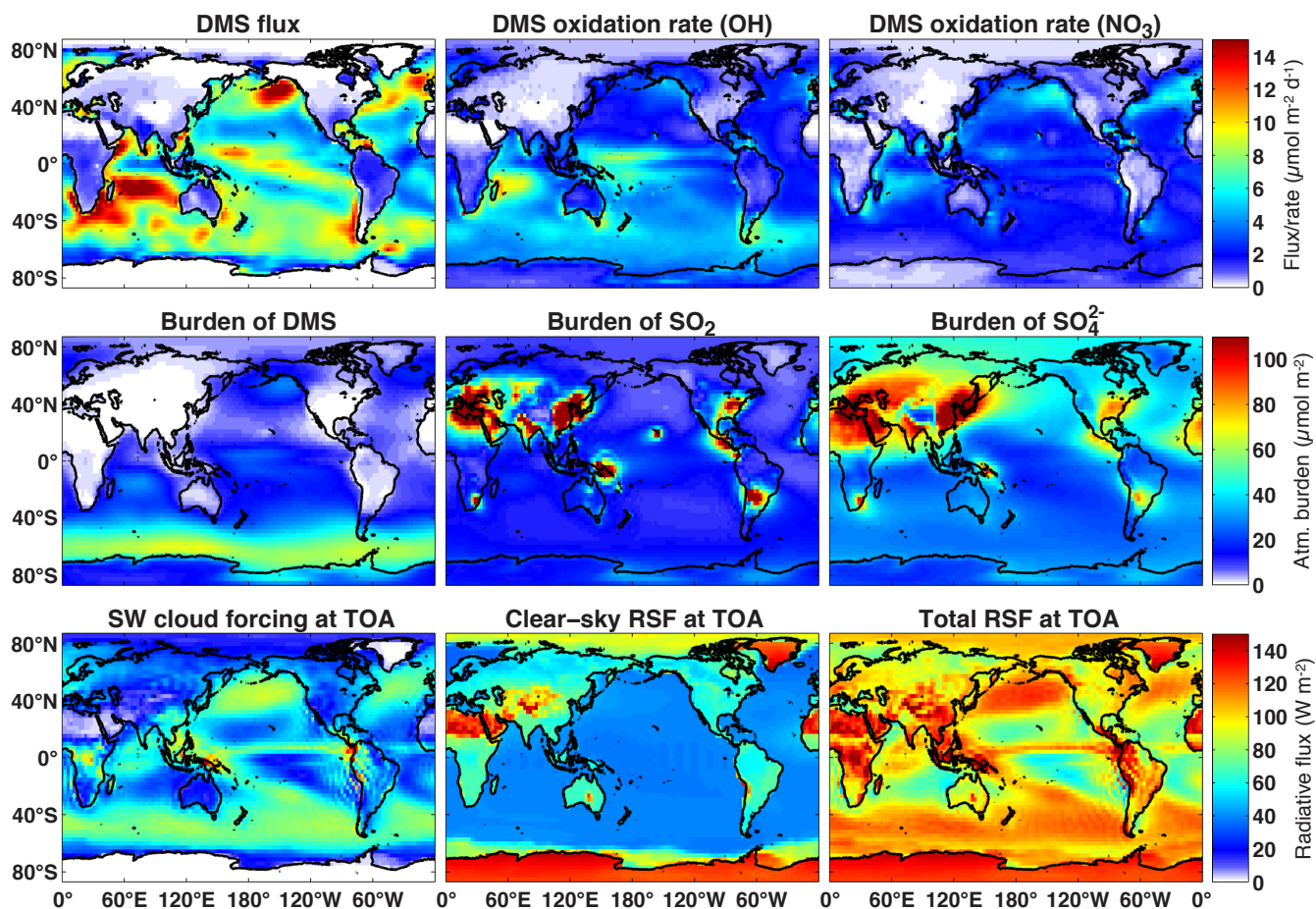


**Figure S1.** Global maps of annual mean distributions of DMS flux, oxidation rates, sulfur burdens and radiation for control run (L10 & N00 &  $\gamma_a$ ). Global maps of flux and oxidation rates of DMS are shown in the upper panels. DMS flux includes terrestrial sources. The only sink for DMS is oxidation to SO<sub>2</sub>, which is shown for both oxidation pathways (oxidation by OH and NO<sub>3</sub> radicals). Global maps of atmospheric sulfur burdens of DMS, SO<sub>2</sub>, and SO<sub>4</sub><sup>2-</sup> are shown in the middle panels. Bottom panels show maps of cloud forcing, clear-sky reflected and total reflected shortwave flux (RSF) at TOA. Total RSF is the sum of cloud and clear-sky RSF.

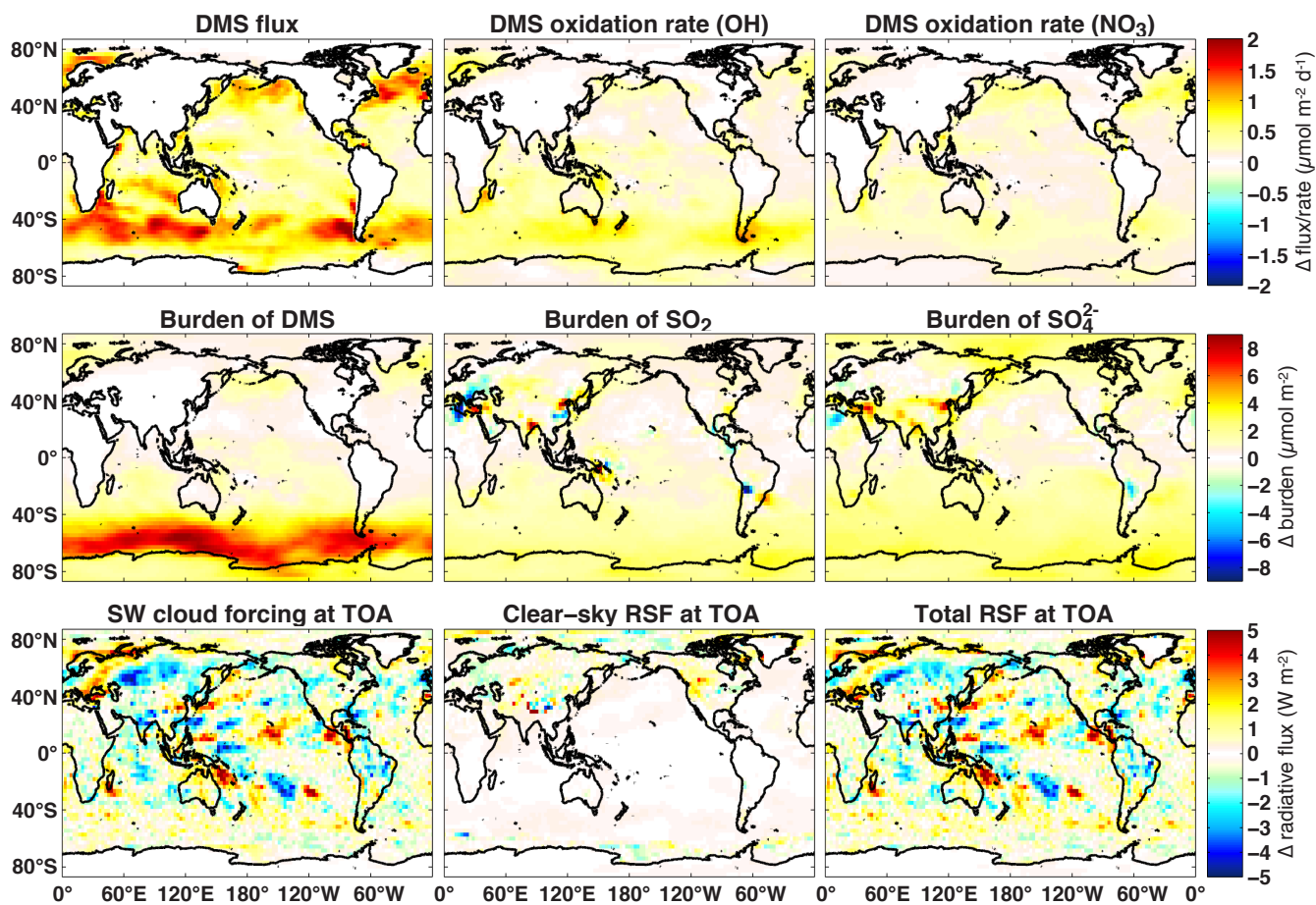


**Figure S2.** Global maps showing absolute differences between model configuration L10 & N00 (control without air resistance) and the control run (L10 & N00 &  $\gamma_a$ ) of DMS flux, oxidation rates (both oxidation by OH and  $\text{NO}_3$  radicals), sulfur burdens (DMS,  $\text{SO}_2$ , and  $\text{SO}_4^{2-}$ ) and radiation (cloud forcing, clear-sky reflected and total reflected shortwave flux (RSF) at TOA). The difference is calculated as experiment run (L10 & N00) minus control run (L10 & N00 &  $\gamma_a$ ).

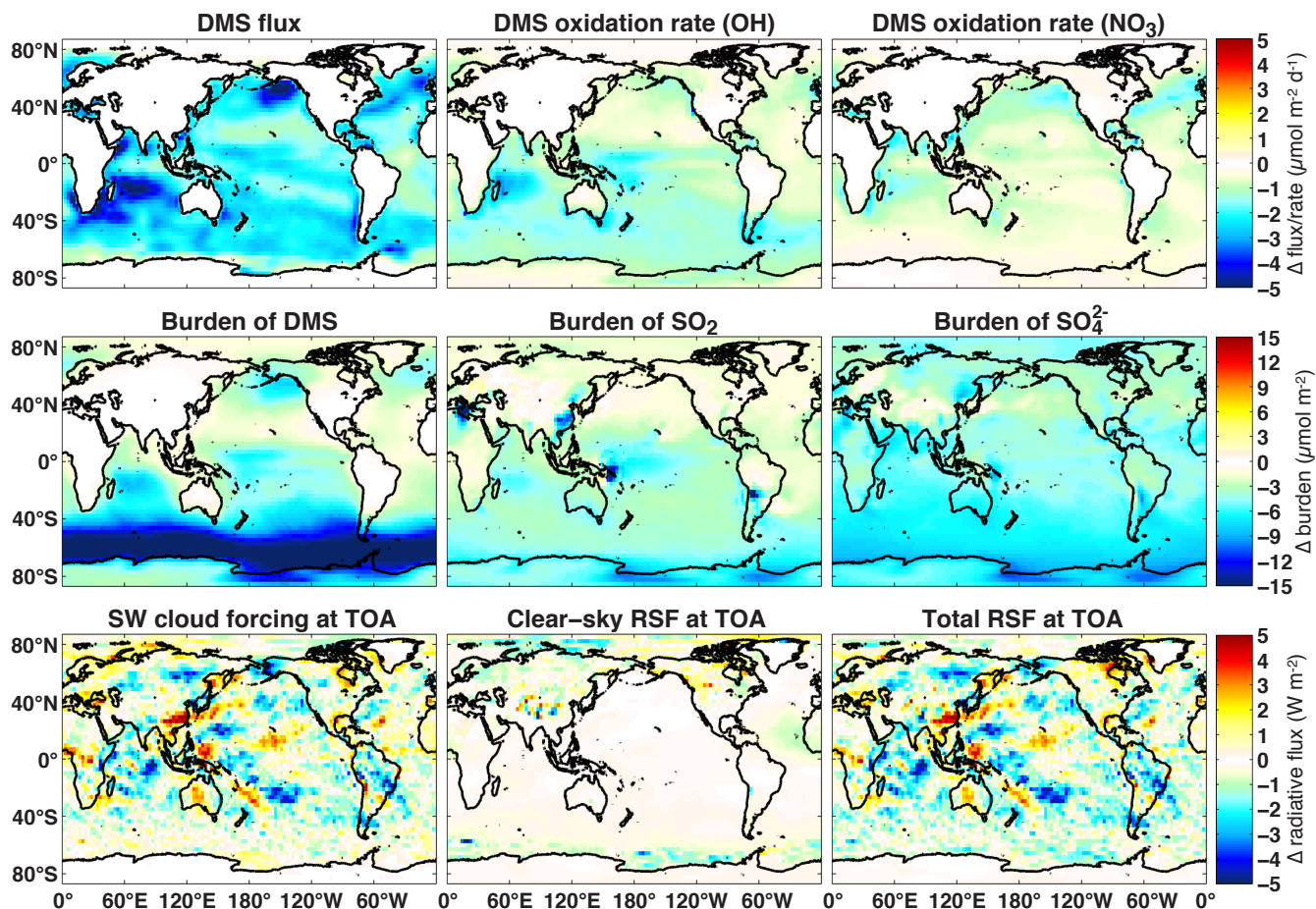


**Figure S3.** Same as Fig. S2, but for experiment L10 & LM86. The difference is calculated as experiment run (L10 & LM86) minus control run (L10 & N00 &  $\gamma_a$ ).

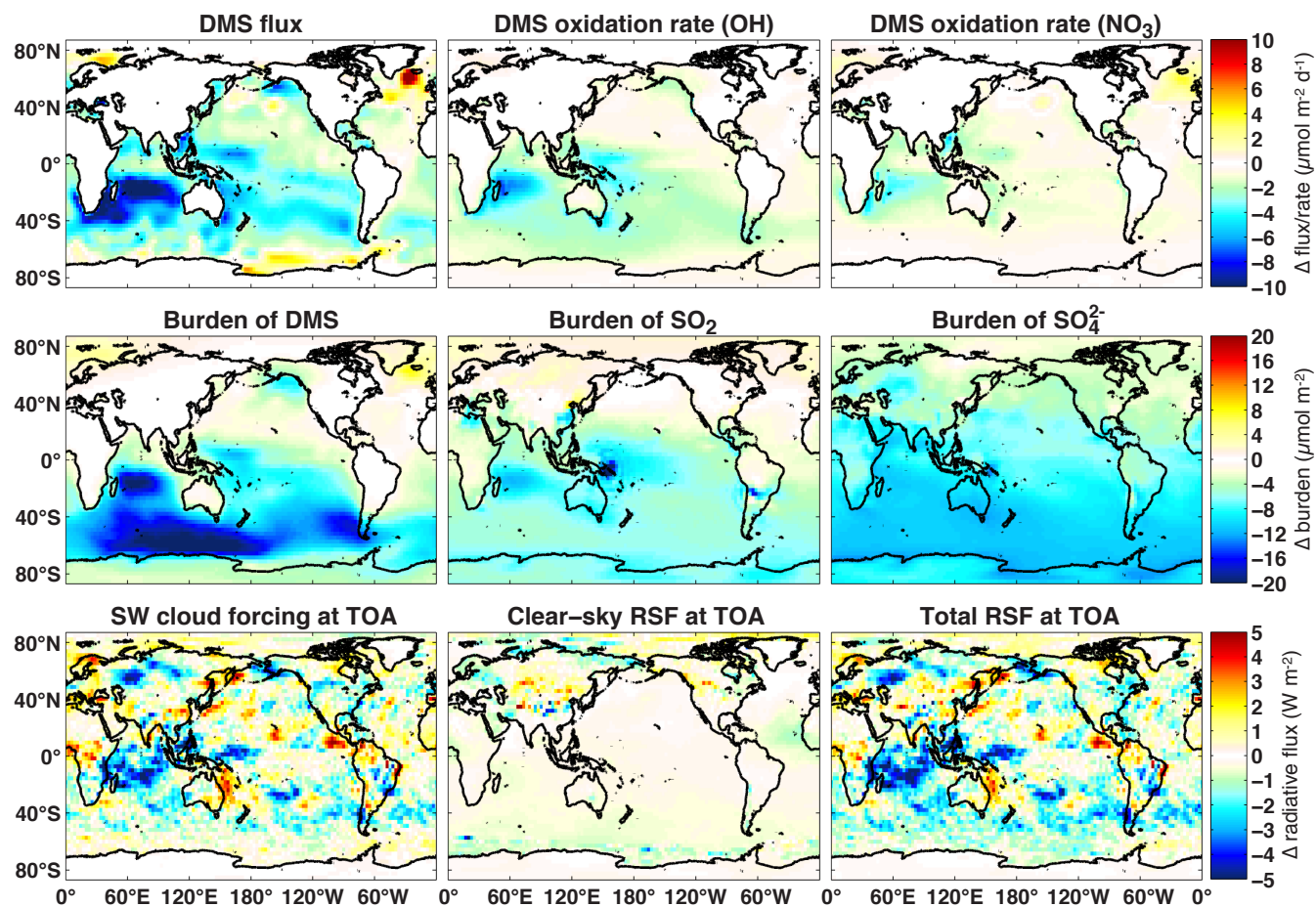


**Figure S4.** Same as Fig. S2, but for experiment K99 & LM86. The difference is calculated as experiment run (K99 & LM86) minus control run (L10 & N00 &  $\gamma_a$ ).

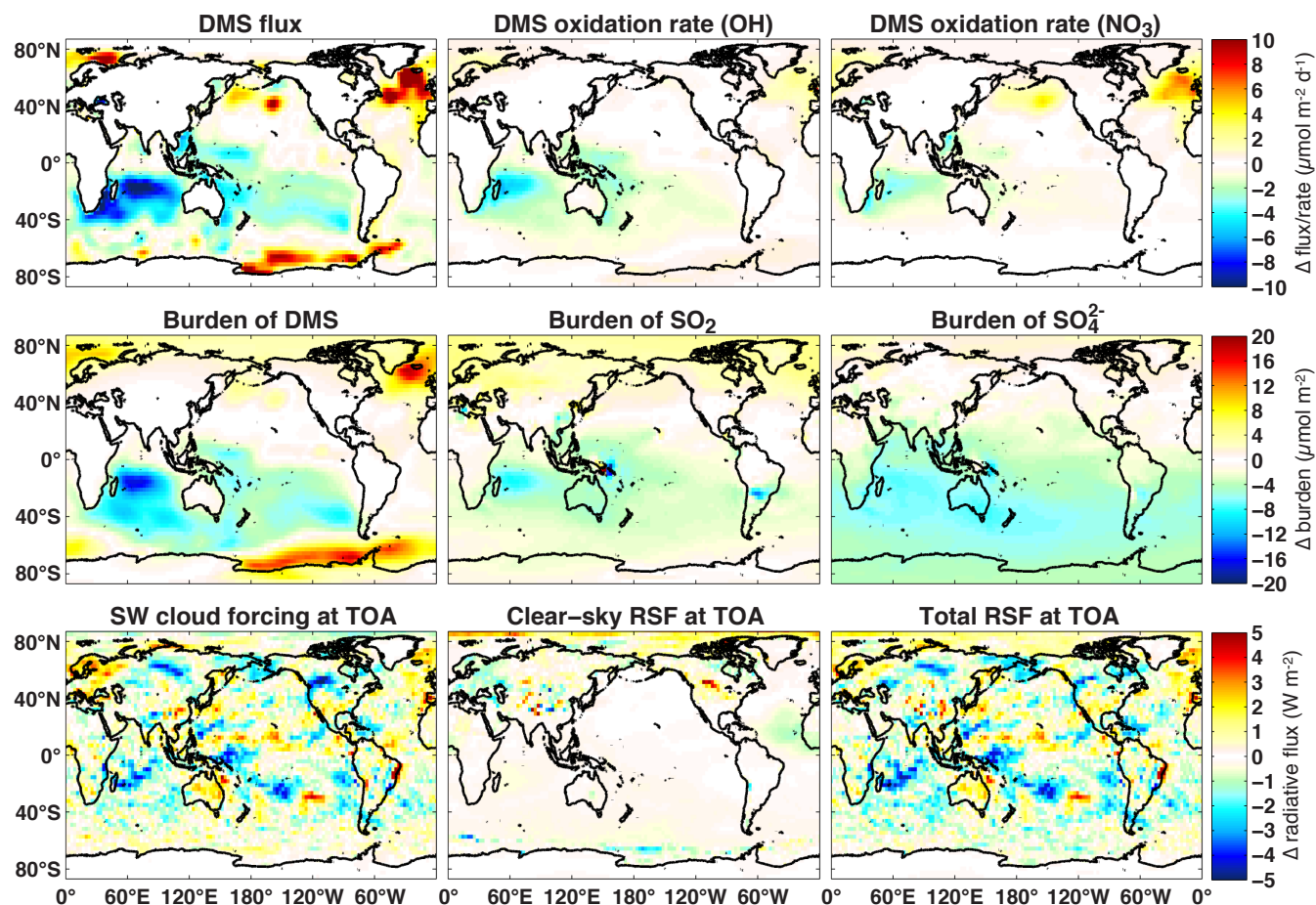


**Figure S5.** Same as Fig. S2, but for experiment K99 & N00 &  $\gamma_a$ . The difference is calculated as experiment run (K99 & N00 &  $\gamma_a$ ) minus control run (L10 & N00 &  $\gamma_a$ ).

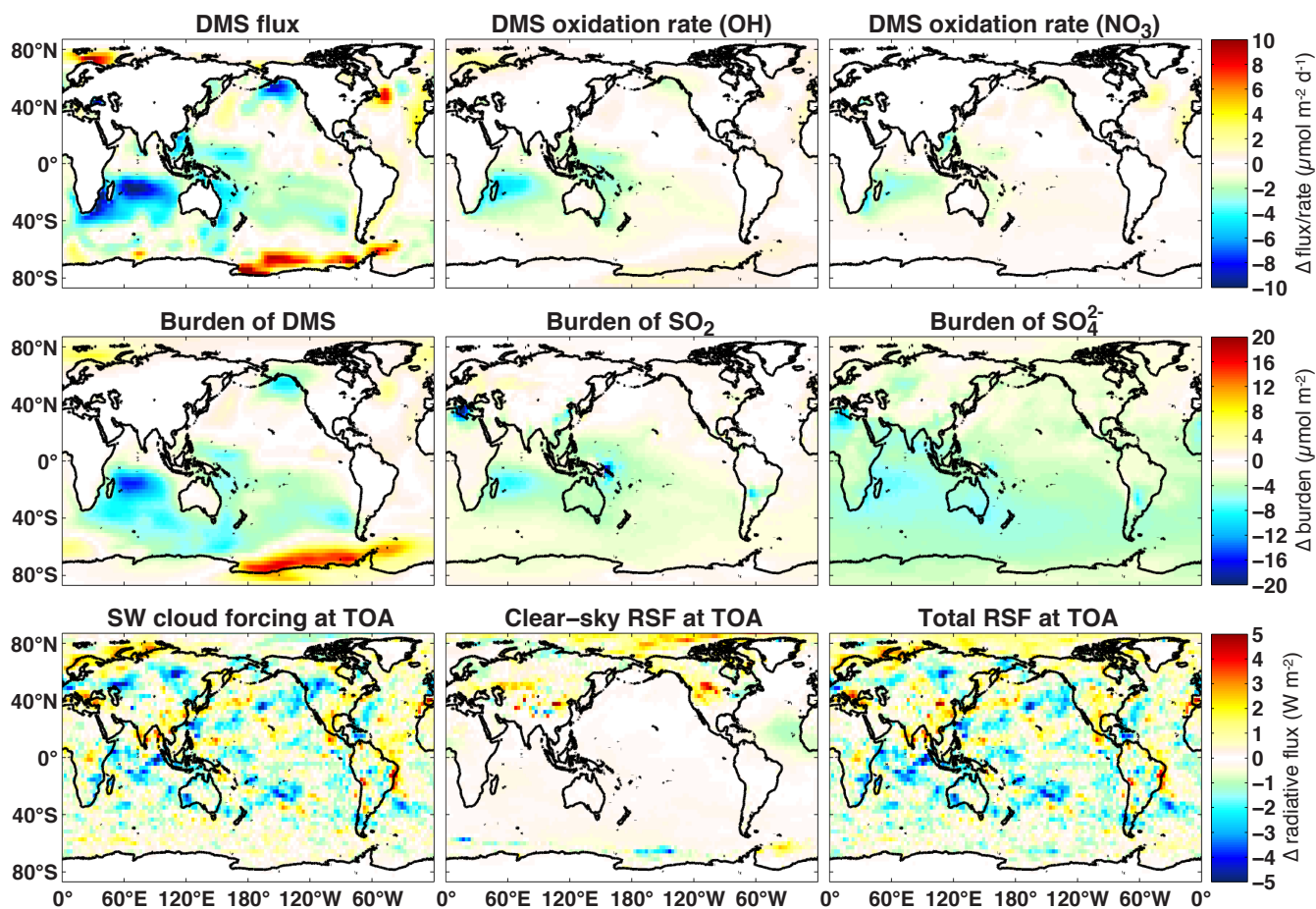


**Figure S6.** Same as Fig. S2, but for experiment K00 & N00 &  $\gamma_a$ . The difference is calculated as experiment run (K00 & N00 &  $\gamma_a$ ) minus control run (L10 & N00 &  $\gamma_a$ ).

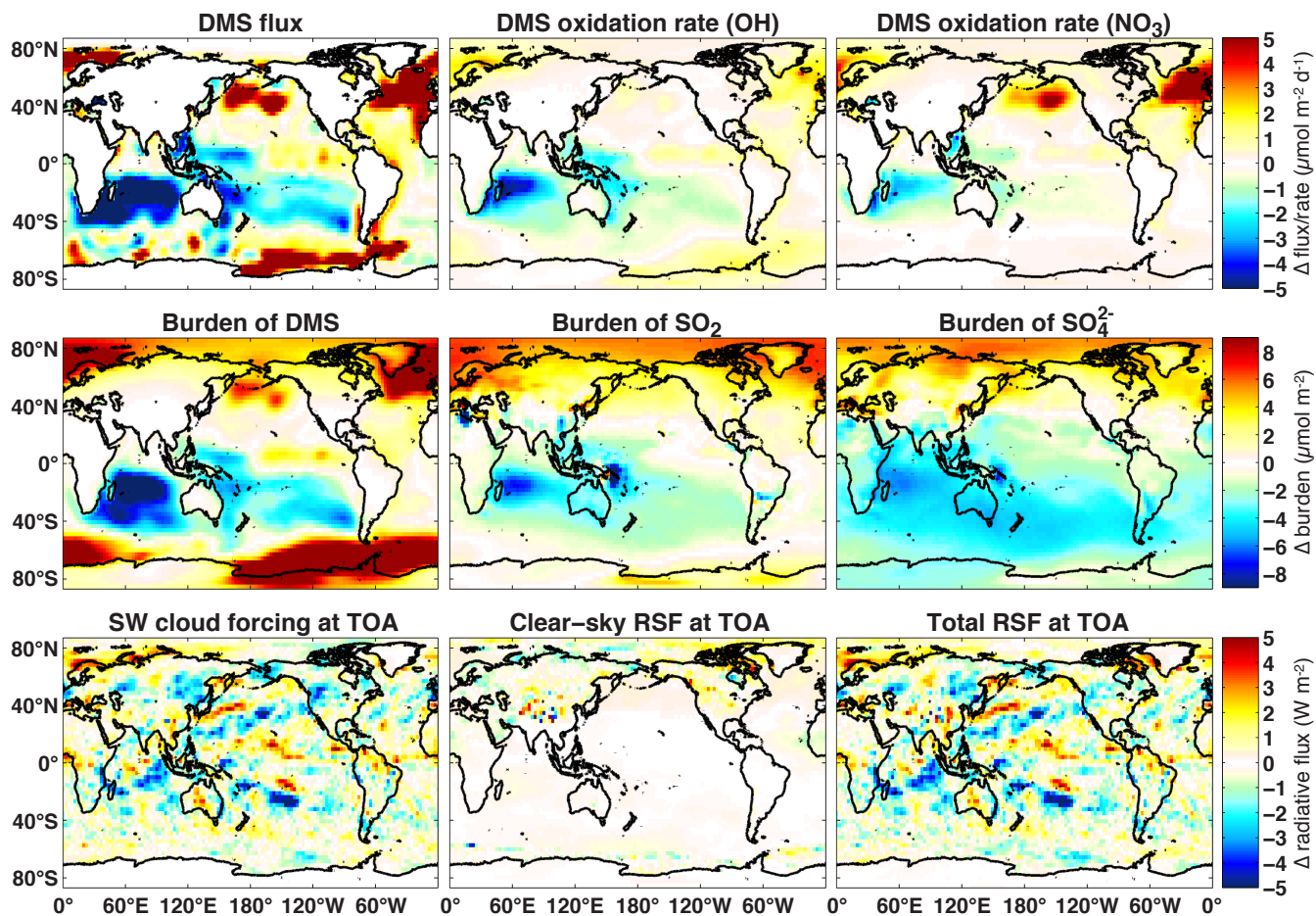


**Figure S7.** Same as Fig. S2, but for experiment K99\* & N00 &  $\gamma_a$ . The difference is calculated as experiment run (K99\* & N00 &  $\gamma_a$ ) minus control run (L10 & N00 &  $\gamma_a$ ).

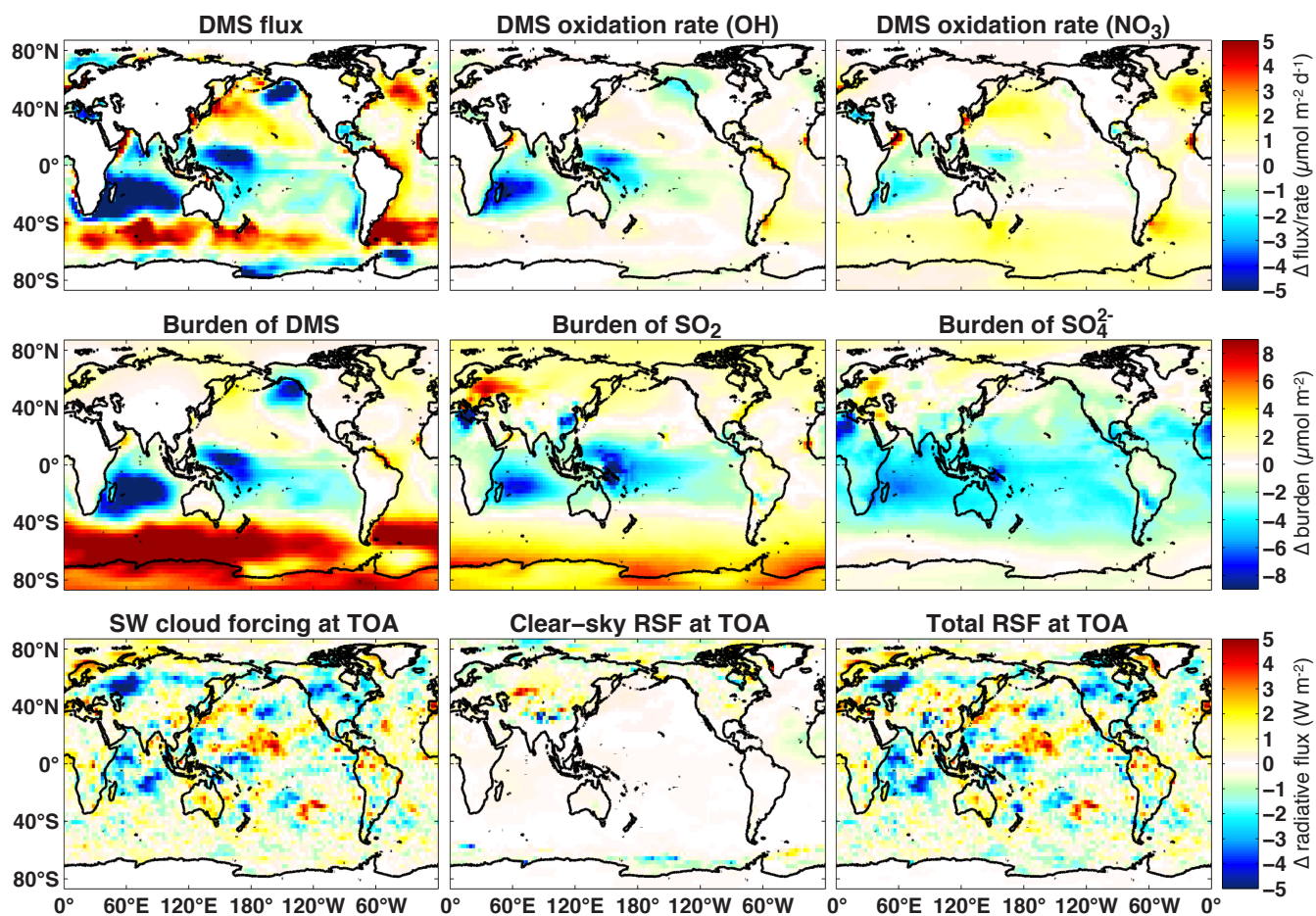


**Figure S8.** Same as Fig. S2, but for experiment AN01\* & N00 &  $\gamma_a$ . The difference is calculated as experiment run (AN01\* & N00 &  $\gamma_a$ ) minus control run (L10 & N00 &  $\gamma_a$ ).

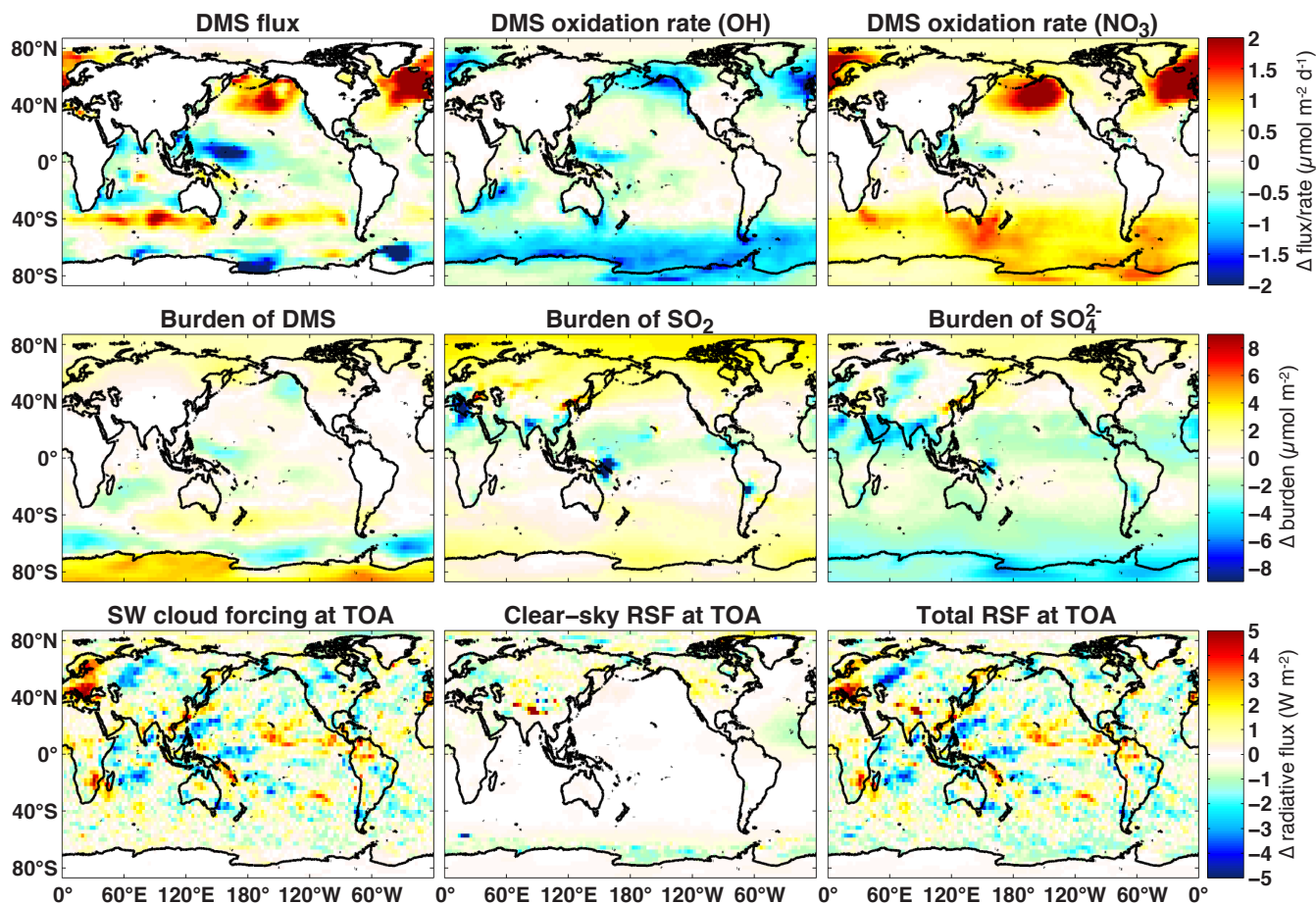


**Figure S9.** Same as Fig. S2, but for experiment using temporally invariant DMS concentration field. The difference is calculated as experiment run minus control run (L10 & N00 &  $\gamma_a$ ).

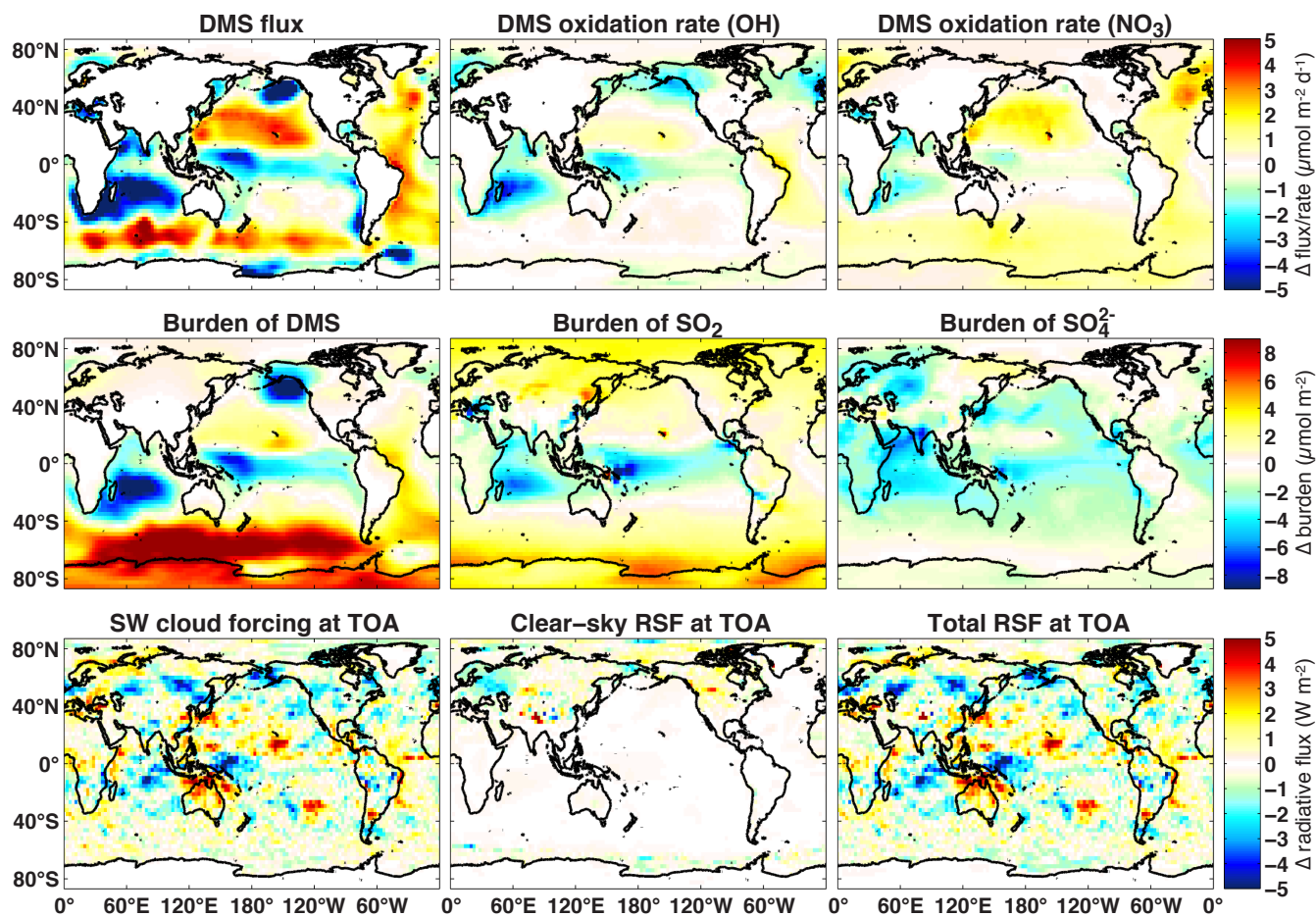


**Figure S10.** Same as Fig. S2, but for experiment using spatially uniform DMS concentration field. The difference is calculated as experiment run minus control run (L10 & N00 &  $\gamma_a$ ).